EACWE 5
Florence, Italy
19th – 23rd July 2009

Flying Sphere image © Museo Ideale L. Da Vinci

A multicamera displacement measurement system for wind engineering testing

F. Fossati, R. Sala, A. Basso, M.Galimberti D. Rocchi
Mechanical Department of Politecnico di Milano – fabio.fossati@polimi.it – Via La Masa 1 20158, Milano – Mechanical Department of Politecnico di Milano – remo.sala@polimi.it – Via La Masa 1 20158 Milano – Mechanical Department of Politecnico di Milano – alessandro.basso@polimi.it – Via La Masa 1 20158 Milano – Mechanical Department of Politecnico di Milano – mario.galimberti@polimi.it – Via La Masa 1 20158 Milano – Mechanical Department of Politecnico di Milano – daniele.rocchi@polimi.it – Via La Masa 1 20158 Milano

Keywords: Wind tunnel, multi-camera displacement measuring system, photogrammetric measurement

ABSTRACT

A new measuring system was developed at the Mechanical Department of the Politecnico di Milano to measure displacements of aeroelastic models during wind tunnel experiments relying on image processing. The system is able to track the variation of the 3D coordinates of model's points that are identified post processing the images recorded by CCD digital cameras using an active stereoscopic vision technique.The measuring system is described in the present paper and some applications to different wind tunnel applications are reported in order to show the system peculiarities and to discuss the advantages of a similar techniques in comparison to other traditional systems.

1. INTRODUCTION

The aim of several wind tunnel tests is the evaluation of the static and the dynamic behaviour of properly scaled models under to wind loads (Diana et al., 2004). That can require to measure the displacements of aero-elastic model's significant points under the wind action without influencing the model dynamic response or the flow. Often, both the static and the dynamic components of the

Contact person: D. Rocchi, Mechanical Department, Politecnico di Milano, Via La Masa 1 20158 Milan, Italy, Tel. +39 02 2399 8485, FAX +39 02 2399 8492. E-mail daniele.rocchi@polimi.it

displacement have to be recorded, during wind tunnel tests, contemporary on several points of the model in order to bound the model shape to the aerodynamic loads or to investigate the dynamic stability at different wind speeds.

This research introduces an innovative optical measurement device which overcomes the typical drawbacks of the instruments that are usually used in wind tunnel tests.

Unlike contact devices it introduces a very weak load effect; it is characterized by a wide measurement range, and, moreover, it allows the contemporary measurement of several points in a single signal acquisition.

The load effect is limited to the adoption of markers helping the detection of interesting point in the image post processing. The dimension and the weight of the markers can be appropriately chosen for each wind tunnel test typology in order to limit the perturbation of the flow and of the mechanical properties of the model under a desired threshold.

The measurement range is linked to the image acquisition settings and to the hardware performances and can be modified in accordance with the peculiar test requirements and measurement uncertainty. Usually, the system offer a wide measurement range and a resolution that can be considered compliant with the wind tunnel tests requirements that often deal with aeroelastic models that are largely deflected by the mean components of the wind loads and oscillate around their static position because of the turbulence fluctuation of the wind velocity and of the wind-structure interaction. These conditions usually are critical in the use of laser transducers.

The possibility to have in a single data acquisition the displacement measure of several points on the model represents indeed an interesting feature for large and slender models whose dynamics and structural deformations are bounded to modal shapes and local effects.

In the first part of the paper a complete description of the measurement system is provided together with the calibration procedure and the system features.

The paper will present, in the second part, some wind tunnel application of the proposed measurement system discussing the advantages of a similar techniques in comparison to other traditional systems.

2. STEREOSCOPIC SYSTEM DESCRIPTION

The system, based on the active stereoscopic vision technique (Trucco et al., 1998; Hartley et al., 2000), is able to measure the 3D coordinates of several points of interest at the maximum frequency of 15 Hz. It is made up of three or more 1/2'' 1392x1040 CCD digital cameras. Greyscale were preferred to RGB cameras, because their resolution is higher and in this application colour information is not required. The GigaEthernet connection guarantees the correct data transmission to the PC that processes them.

Each camera is equipped with a 8-48 mm variable-focus lens. This was preferred to a set of interchangeable lenses in order to be able to quickly modify the measurement volume. Photographic heads were used to constrain the cameras to the wind tunnel walls. It is very important to pay a great attention to perform a steady constrain in order to avoid the system to vibrate because of the wind turbulence. Each camera is also equipped with a coaxial high intensity infra-red LED circular array, activated by means of a trigger signal, which synchronizes the lighting and the image grab.

The stereoscopic measurement technique is based on the fact that a point in the scene, acquired by means of two (or more) cameras placed in different positions and with different poses, occupies different positions in the images (Trucco et al., 1998; Hartley et al., 2000).

Image formation can be modelled as a geometric projective process: it means that if a phisical point is projected onto a particular point in a camera sensor (i.e. it has a particular position in the image), the same point cannot be projected anywhere in another sensor, but it has to lie on a straight line, called epipolar line (due to the measurement noise the epipolar line actually becomes a stripe). All other points belonging to the image but not to the epipolar stripe can be filtered out in the correspondence search. The points in different images that identify the same physical point are called

corresponding points. If the camera interior and exterior parameters are known as well as the corresponding point positions in the images, it is possible to determine the 3D coordinates of the point they represent. All cameras must be properly synchronized, because the analysis of images taken at different times generally leads to wrong results.

The main difficulty to make the measurement process fully automated is the capability to recognize the corresponding points without the interaction of an user. This is why our system has three cameras placed on the vertices of a triangle: two of them are used to actually perform the 3D measurement, the third one to implement an effective filter, based on the epipolar geometry, able to automatically associate the corresponding points (Hartley et al., 2000). The third camera could be also useful to make the measurement more robust, but at this stage of the research it is only used for the point association task.

The measuring system is controlled by a software that is developed at the Mechanical Department of the Politecnico di Milano. The developed software deals with both acquisition and image processing stages, allowing users to carry out on-line analysis. The first part of the analysis consists in performing the blob detection of all the acquired images (Gonzales et al., 2004). In this way the positions of the interesting points are determined in the images. Then the corresponding points are automatically found by means of the epipolar filter and eventually the 3D coordinates of all the points of interest are computed.

The procedure is repeated on each frame of the camera acquisition leading to the reconstruction of the time histories of the 3 components of the position of each point at different time steps.

3. STEREOSCOPIC SYSTEM CALIBRATION AND UNCERTAINTY ANALYSIS

The calibration of the system is performed by acquiring several points evenly spaced in the measurement volume whose 3D world coordinates are well-known (Zhengyou Z., 1998). To this purpose a calibration frame is designed and built. The calibration frame is made up of a 910x910 mm^2 planar structure with 16 spherical markers evenly spaced in four rows and four columns, diameter 20 mm, coated with a reflective tape. Several images are taken, while the frame is moved in well-known positions along a prismatic slide perpendicularly to the frame itself. The three cameras are calibrated at the same time in order to avoid introducing a further uncertainty source due to the registration procedure.

The metrological performances of the system were assessed in accordance with the Guide to the Expression of Uncertainty in Measurement (GUM) (ISO, 1995). The whole uncertainty is due to two main sources: one is introduced by the calibration procedure, the second by the measurement system itself.

On one hand, the calibration procedure introduces two contributions to uncertainty. The first one is related to unavoidable discrepancies between the actual and the expected marker positions in the calibration frame. Its magnitude depends on the quality of the machine tools used to manufacture the calibration frame. The second source is the slide that moves the frame.

Let us define x and y the axes that identify the calibration frame, while z corresponds to the direction along which it is moved. The related uncertainty values are:

$$u(p_X) = 0.02\,mm; \qquad u(p_Y) = 0.02\,mm; \qquad u(p_Z) = 0.05\,mm \tag{1}$$

The calibration uncertainties along the x and y axes are:

$$u_{X,cal} = u(p_X) = 0.02\,mm; \qquad u_{Y,cal} = u(p_Y) = 0.02\,mm \tag{2}$$

The combined calibration uncertainty along the axis z is:

$$u_{Z,cal} = \sqrt{u^2(p_z) + u^2(s_z)} = 0.07\,mm \tag{3}$$

On the other hand the uncertainty due to the vision system is mainly caused by the discretization

introduced by the sensor pixel structure. Sub-pixel algorithms were used in order to increase the accuracy of the marker centre estimate in the images. The actual resolution depends on the marker size: the bigger is the marker, the better becomes the resolution. Tests carried out during calibration showed that a resolution of one tenth of pixel was attained. The system layout affects the overall uncertainty too, in particular the baseline, the camera orientations with respect to the baseline and the optical focal lengths (i.e. the zoom value). It follows that in each experimental campaign it is fundamental to set a trade-off between measurement volume and uncertainty.

The uncertainty study is performed considering the couple of cameras that are actually used to perform the 3D measurement. It is worth remembering that the third camera is only used for the automatic corresponding point association. The uncertainty value clearly depends on the system setup: in the following we show as an example the results related to the tests performed on a bridge deck section model that will be presented in 4.2.

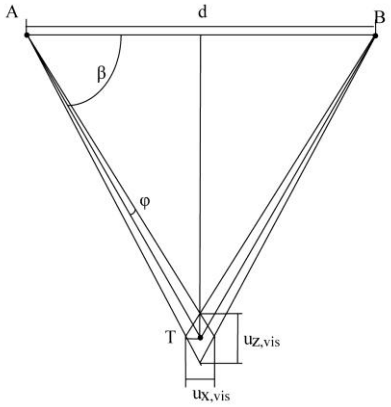

Figure 1: Analysis of the uncertainty introduced by the discretization of the camera sensors.

In Figure 1, A and B represent the camera optical centers, d is the baseline, β is the camera orientation with respect to the baseline and φ is the angle identifying the uncertainty related to the image marker's centre computation. This figure shows the effect of the camera sensor discretization in the measurement of the 3D position of a point of interest.

Baseline [mm]	1000
Camera orientation with respect to the baseline [°]	70
Optical focal length [mm]	20
Horizontal resolution CCD [pixels]	1392
Vertical resolution CCD [pixels]	1040
Sensor width [mm]	6.4
Sensor height [mm]	4.8
Pixel size [μm^2]	6.45x6.45

Table 1 Example of system setup values

$$u_{x,vis} = u_{y,vis} = \frac{d}{2 \cdot \sqrt{3}} \cdot \frac{tg(\beta) - tg(\beta - \varphi)}{tg(\beta - \varphi)} = 0.03 mm \tag{4}$$

$$u_{z,vis} = \frac{d}{4 \cdot \sqrt{3}} \cdot \left[tg(\beta + \varphi) - tg(\beta - \varphi) \right] = 0.07 mm \tag{5}$$

According with

Figure 1 and Table 1:

$$\varphi = arctg\left(\frac{0.1 \cdot pixel\_size}{focal\_length}\right) \tag{6}$$

The overall extended uncertainty is obtained by combining the calibration and the vision system uncertainties:

$$u_{X,tot} = 3 \cdot \sqrt{u_{x,cal}^2 + u_{x,vis}^2} = 0.12\ mm\ (LC\ 99.7\%, cf = 3) \tag{7}$$

$$u_{Y,tot} = 3 \cdot \sqrt{u_{y,cal}^2 + u_{y,vis}^2} = 0.12\ mm\ (LC\ 99.7\%, cf = 3) \tag{8}$$

$$u_{Z,tot} = 3 \cdot \sqrt{u_{z,cal}^2 + u_{z,vis}^2} = 0.30\ mm\ (LC\ 99.7\%, cf = 3) \tag{9}$$

4. MEASURING SYSTEM APPLICATIONS

Hereafter will be reported some examples of the application of the measuring technique to wind tunnel tests performed in the Politecnico di Milano wind tunnel. Initially will consider tests where the goal is the definition of the model static displacement and then an application where both the static and dynamic components are important.

4.1 Sails.

From a strictly aerodynamic design point of view, a sail is a rather complex system to study since sails have a variable shape, both because the material deformation and the trimming performed by the crew under sailing, making the problem typically aeroelastic.

Even though the sail design shape is essentially known, it is still not easy predictable the final flying shape and its relevant influence on the final yacht performance. Furthermore the contemporary measure of the actual sail shape with the instantaneous force acting on the boat at different wind conditions represent a challenging matter that is faced by different authors through full scale measurements (Masuyama Y. et al, 2007; Milgram J. et al, 1993), numerical approaches (Krebber B. et al., 2006) or wind tunnel tests (J. M. C. Campbell et al., 1994; R. G. J. Flay, 1996 and Fossati F. et al., 2006). Wind tunnel tests on scale models are decidedly more attractive, both for economic reasons and because they permit to work in controlled conditions compared to real life condition that implies very high costs and potential results scattering due to environmental and meteorological effects.

Wind tunnel tests were performed in twisted flow on a complete 1:10 scaled model of a 48’ IMS cruiser-racer sailing yacht, consisting of yacht hull body (above the waterline) with deck, mast, rigging and sails, mounted on a six component force balance, which is fitted on the turntable of the wind tunnel used to tests different apparent wind directions (Figure 2 left)

The tested sailplan is a typical IMS type sailplan for upwind conditions: in particular a mainsail with the maximum IMS rule allowed roach and 100% non overlapping jib have been used.

The sheet trims are controlled by the sail trimmer who operates from the wind tunnel control room through a radio controller.

High reflective markers (8 mm diameter) are glued on 8 horizontal sections of each sail plus one on the top, on both windward and leeward side (Figure 3 left). On each of the mainsail sections there are six markers, and on the jib sections markers are 7: concerning targets on the jib at different

heights, 6 of them are equally spaced, and the seventh is halfway between the first and the second marker on entry angle at the luff, to acquire the most accurate changes in curvature.

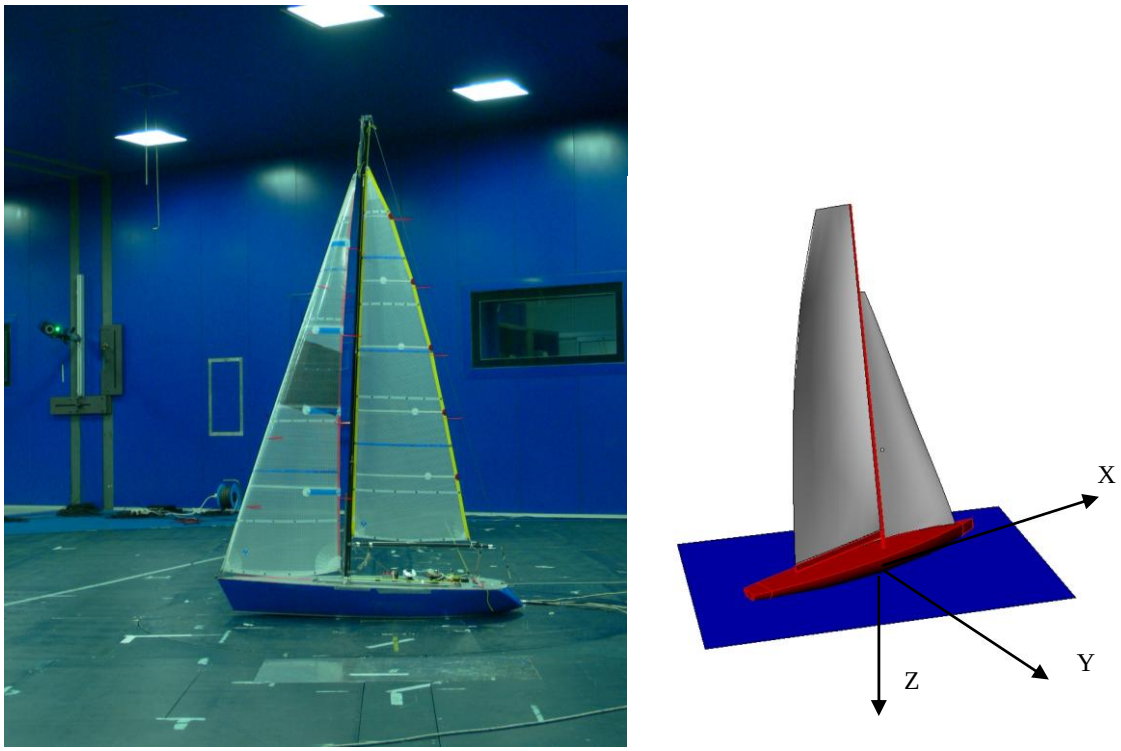

Figure 2: Sailplan tested in wind tunnel (left) and force reference system (right).

In order to overcome difficulties arising from sails overlapping especially in downwind configurations and in order to be able to have at least three useful points in each part of the sails the system is equipped with five cameras.

Once obtained the cloud of points from the multicamera system, representing the position of the markers during the tests, the flying shapes is reconstructed by fitting the data in order to evaluate maximum camber, maximum draft position and twist on four sections at fixed height for each sail.

For each sail the 3D points array is fitted with a cubic spline over each horizontal section, with the aim of calculating a new pattern of points, dividing each curve in 5 equal parts. Therefore, cloud of points of two sails are fitted in vertical sense with cubic splines, building six curves for the mainsail and seven for the jib, starting from the top point, ending on the sail foot and passing through points in between, as shown in Figure 3 on the right.

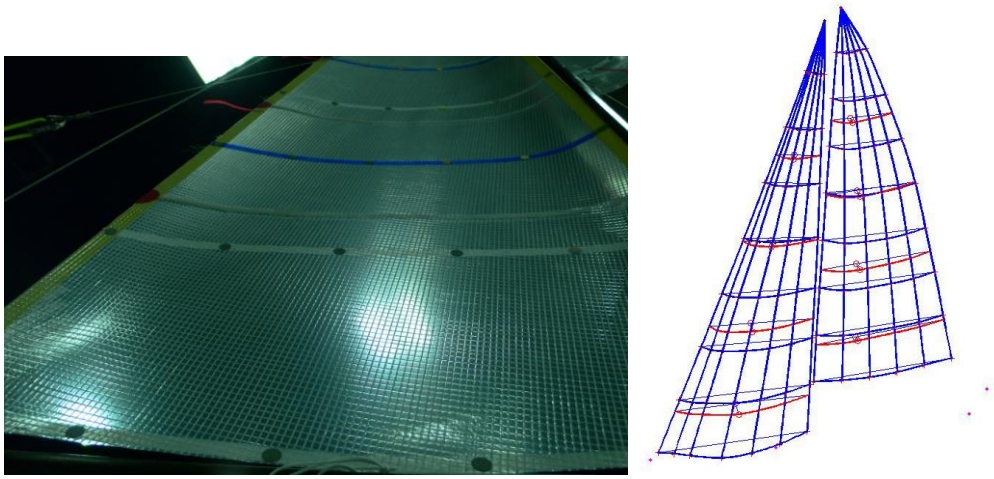

Figure 3: Reflective markers on the main sail (left) and flying shape surface modeling and parameters extractions (right).

Four different sections of sails have been considered at 10% 30% 50% and 70% height of P and I for mainsail and jib respectively.

For each section following parameters have been evaluated (Figure 4):

- maximum camber (% of chord length)
- maximum draft position (% of chord length)
- twist angle (referred to boat centreline)

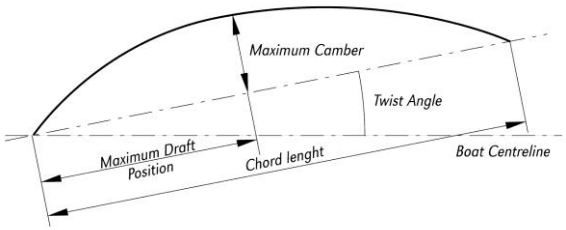

Figure 4: Measured sail shape parameters

The twist angle of the boom is evaluated using two markers respectively placed at the boom gooseneck and at the aft end considering the yacht centreline as the reference line and the jib foot twist angle (from the centreline) has been also evaluated.

The aerodynamic loads were measured by the force balance embedded in the model and a correlation between sail shape and wind loads is possible.

As an example the variation of the driving force coefficient C_x and of the heeling force coefficient C_y with mainsail camber, computed as the mean value of the maximum draft of four considered sections of the mainsail at different mast height mainsail, is shown in Figure 5 on the left.

The variation of the same quantities with mainsail maximum draft position i.e. the mean value of the four considered mainsail sections at different mast height is reported in Figure 5 on the right.

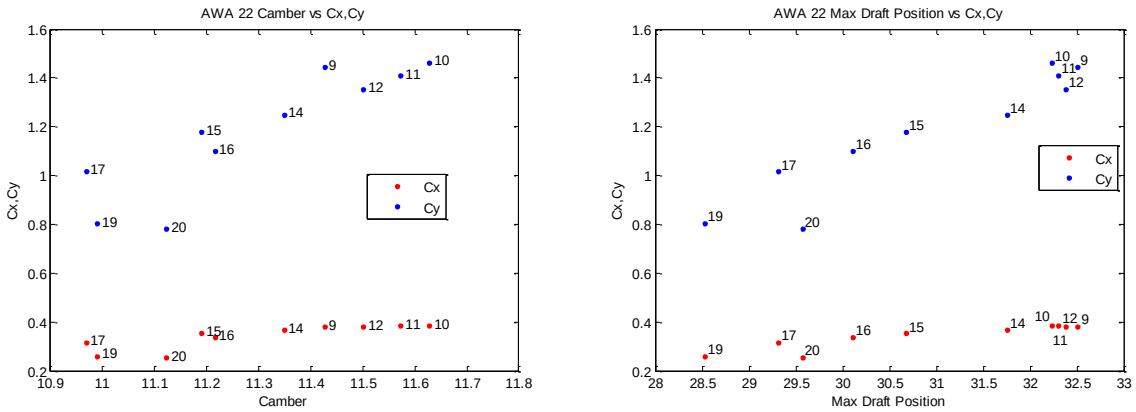

Figure 5 Drive and heeling force coefficients vs camber (left) and vs maximum draft position (right).

4.2 Bridges.

Bridge aeroelastic stability is usually evaluated through wind tunnel tests on elastically suspended deck models (Diana et al., 2004) or on full aeroelastic models (Cheli et al., 2007), or by using

numerical computations relying on the bridge deck aerodynamic coefficients (Johns et al., 1998).

To study the behavior of the bridge deck under wind loads it is needed to measure the displacement of the bridge model at different wind speed to identify vortex shedding or instability phenomena. Using full aeroelastic models the whole bridge structure is reproduced, and different deck sections along the bridge axis show different static and dynamic contributions. Usually instrumentation is placed taking into account the antinode positions of the first modal shapes involved in the motion in order to limit the number of transducers that increase the complexity of the measurement chain and locally alter the model structural characteristics and the local flow. Multi axial accelerometers are usually used to have information on the 3D motion using a single transducers. The multicamera system overcome these restrictions limiting the load effect to the positioning of the very small and light markers that allow to rebuild the 3D displacement of a large number of sections.

Using rigid deck sectional models, elastically suspended in the wind tunnel has the advantage to work with larger models and higher Reynolds numbers. The load effects are less important and the behaviour of a single deck section of the bridge is considered transferring to numerical approaches the definition of the full bridge response.

Nevertheless, both with full aeroelastic models and with suspended rigid models, the definition of the aeroelastic response shows the complexity to measure both the static and the dynamic components of the displacement. Increasing the wind speed the static equilibrium position of the deck model will change accordingly to the aerodynamic mean forces and the dynamic response of the bridge deck will depend on the angle of attack between bridge and wind. Depending on the aerodynamic characteristics of the deck sections the static position and the oscillations may be large and a measuring system with a large measuring range is required.

As an example some results of a wind tunnel campaign on a rigid deck sectional model of a cable stayed bridge, using the multicamera system are hereafter reported.

The deck sectional model (3m long and 1 m wide) was elastically suspended in the wind tunnel tests section and was equipped with 10 markers positioned at 4 different sections along the bridge axis, as illustrated in Figure 6. Four markers were placed in the row closest to the acquisition system (the edge on the right in Figure 6), in order to perform a more valuable analysis in the measurement volume part where the uncertainty is expected to be the lowest.

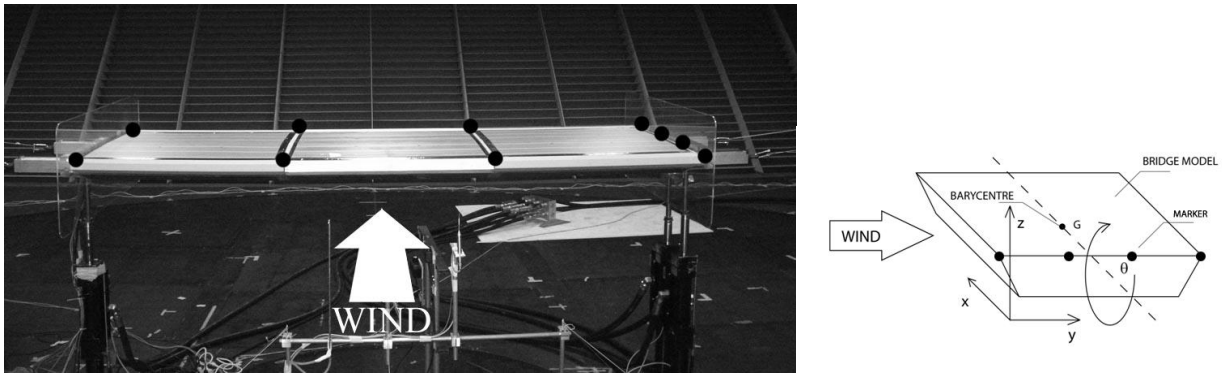

Figure 6: Marker (identified with the black dots) positioning on the bridge model

Tests were performed in nominal smooth flow (turbulence intensity less than 2 %) at different wind speeds. By the reconstruction of the positions of the different markers belonging to the same section it is possible to evaluate the angle of attack and the vertical and lateral position of the whole model, and by the availability of the same information on different deck sections along the bridge axis a check on the 2 dimensionality of the test is feasible.

In Figure 7, the dependence of the angle of attack with the wind speed is reported together with the vertical and lateral position according to the sign convention of Figure 6 (right).

As an example, in Figure 8, a typical aerodynamic instability situation is shown. Results are referred to a 8 m/s wind speed test where the mean angle of attack reaches almost 5 deg. The figure reports on the left the pitch time histories and on the right the horizontal displacement. As can be seen

vibration amplitudes increase rapidly due to the aerodynamic instability and, as shown in the figures, during the tests the bridge model was manually stopped in order to avoid any damage.

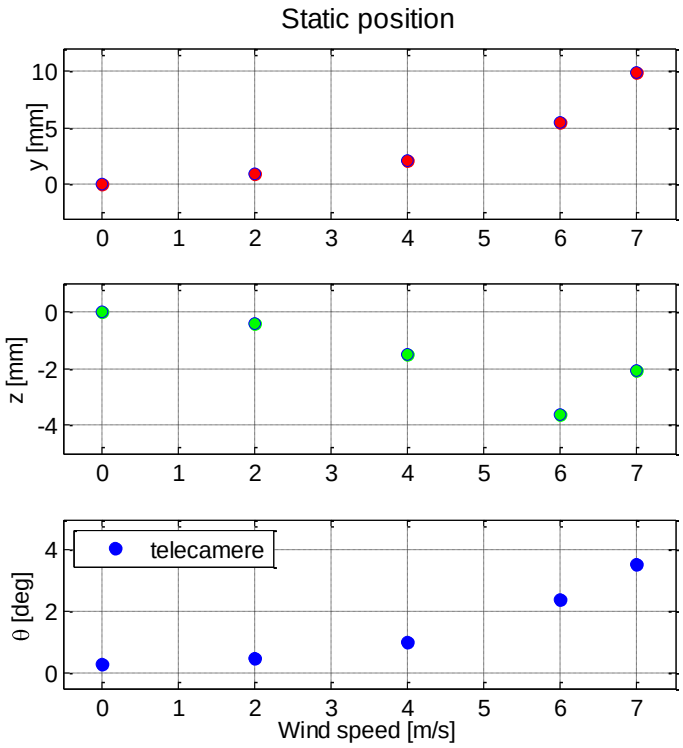

Figure 7: (a) pitch angle – (b) horizontal displacement

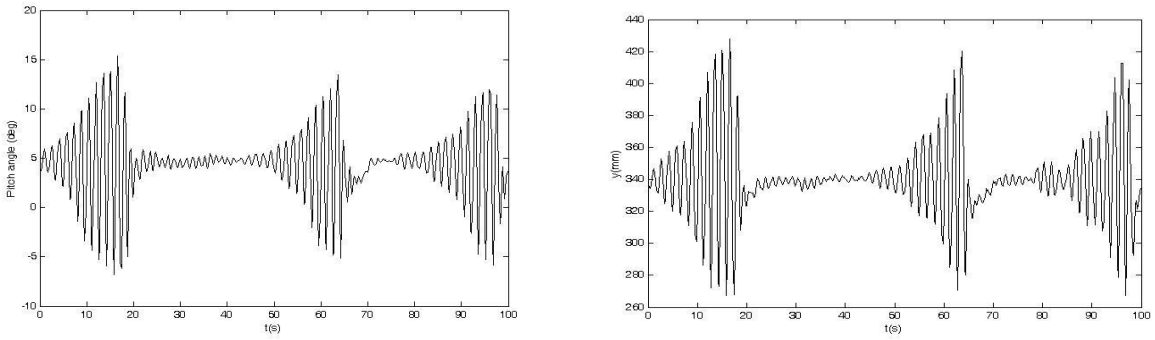

Figure 8: (a) pitch angle – (b) horizontal displacement

4.3 Over Head Line.

A wind tunnel investigation has been performed to study the fluctuation induced by the wind on a Over head power line (OHL) positioned in the wake of a wind turbine.

A 1:50 scale model of a 3 MW wind turbine has been built with the possibility to control the angular speed of the rotor and the blades pitch angle.

An aeroelastic model of an OHL was designed and built in the same 1:50 geometrical scale reproducing the dynamic characteristics of an Araucaria 400 m long span cable with a maximum sag span of 15 m. Due to the low scale ratio the diameter of the aeroelastic cable model is 0.75 mm with a mass per unit length of 1.1 g/m. It is therefore mandatory to use a measurement system with a load effect as low as possible in order to not modify the model dynamic behavior.

The cable dynamic response was studied by means of the measurement of the spatial displacement of some cable points of interest equipped with markers using the multicamera system. The positions of the markers (named “a”, “b”, “c”, “d” and “e”) along the cable and the reference frame adopted for the data post processing are reported in Figure 9.

The comparison among the first natural frequencies of the full scale OHL, the expected natural frequencies obtained applying the aero elasticity scaling rules and those obtained by a structural parameter identification on the wind tunnel model in still air is reported in Table 2. The natural frequencies identification was performed studying the free cable vibration starting from imposed generic initial conditions and analyzing the decay of the vibration amplitudes of the 5 examined points. Figure 10 reports the spectra of the decay time histories of the considered points along the cable where the peaks in correspondence of the natural frequency are clearly visible and it can be appreciated the antinode position of “marker c” for the second and fourth mode shape.

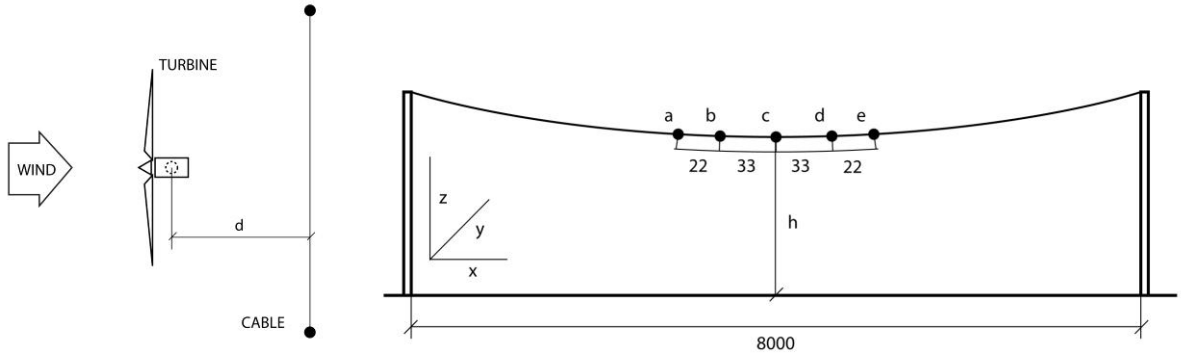

Figure 9: Wind turbine and aeroelastic cable model relative position (left, view from the top) - Marker position and reference frame (right, view from the front).

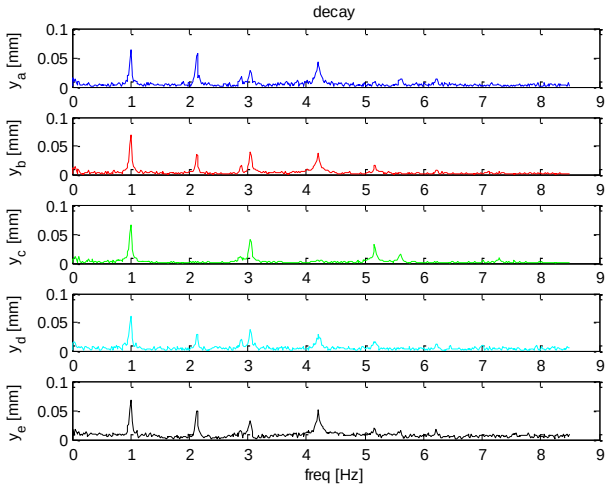

Figure 10: Spectra of the lateral displacement

Natural freq.	Full scale [Hz]	Expected [Hz]	WT model [Hz]
1	0.14	0.98	0.96
2	0.28	1.98	2.12
3	0.42	2.96	2.89
4	0.56	3.95	4.19
5	0.71	5.02	5.01
6	0.84	5.93	6.19
7	0.99	7.00	7.11
8	1.13	7.99	8.4

Table 2 Natural frequencies of the full scale OHL and of the wind tunnel model

Tests were performed in turbulent flow conditions, reproducing an atmospheric boundary layer profile by means of passive turbulence generators. Different relative positions *d* between the OHL model and the wind turbine (Figure 9) and different line heights from the ground have been taken into account. The dynamic response to turbulent wind of the OHL in free stream was also measured and taken as reference.

Figure 11(left) shows the time histories of the 3 components of the displacement of "marker a" during a wind speed start up from 0 m/s to 2.8 m/s. The lateral and vertical components show how the cable change its position and start oscillating around a new mean deformed configuration and how the measurement system is able to contemporary measure both the contributions.

Figure 11(right) reports another representation of the OHL model response during a transient change of the wind speed from 0 to 1.4 m/s where the trajectories of the 5 markers are plotted in a 3D reference frame.

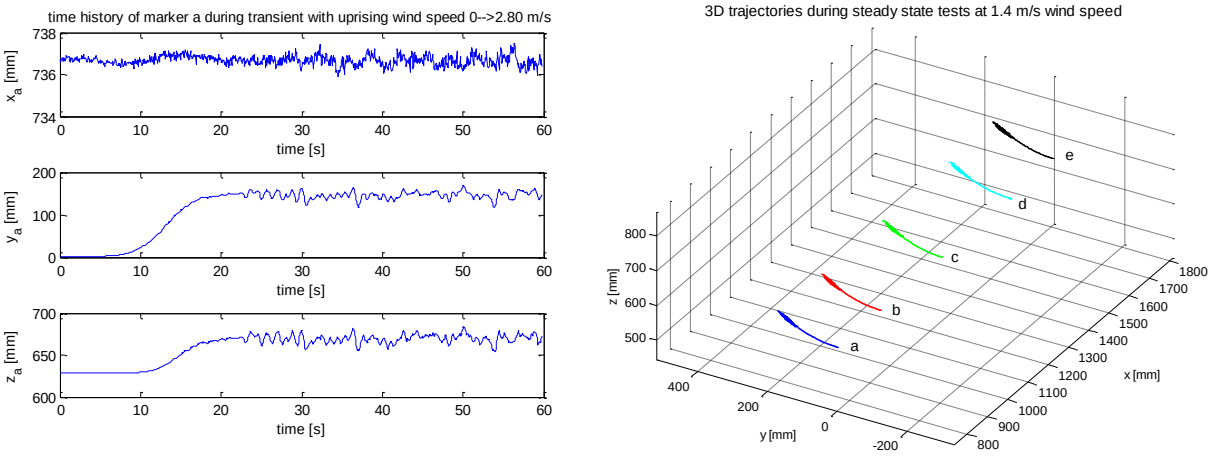

Figure 11: Wind turbine and aeroelastic cable model relative position (left, view from the top) - Marker position and reference frame (right, view from the front).

As final example, in Figure 12, the mean value and the standard deviation of the y displacements of the five markers are reported for different operating condition at a wind speed equal to 2.12 m/s. It is possible to observe, comparing the case without the wind turbine against the others, that both the mean displacements and the standard deviation along the wind direction are larger when the wind turbine is put upwind the cable model.

The multicamera system allowed to measure the cable static and dynamic response of the OHL model for different relative positions between wind turbine and cable model highlighting a dependence of the vibration amplitudes from the position due to an interaction with the wake produced by the wind turbine.

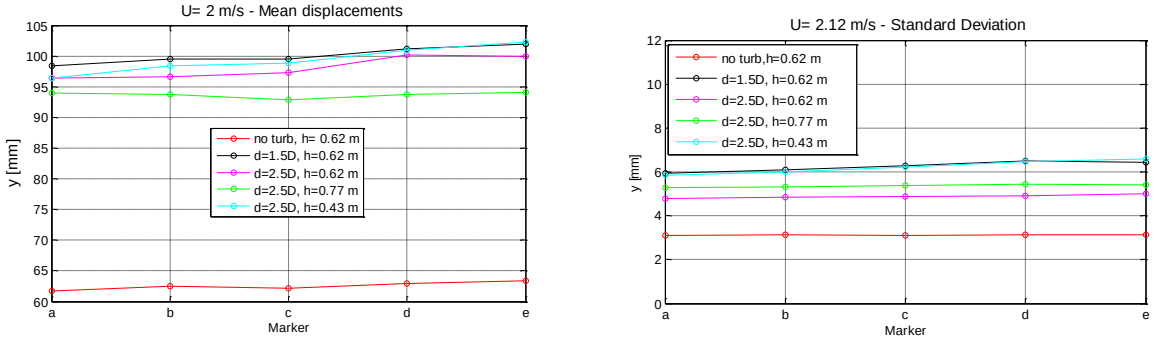

Figure 12: Mean value and standard deviation of the y displacement of the markers

REFERENCES

G. Diana , F. Resta , A. Zasso , M. Belloli and D. Rocchi, Forced motion and free motion aeroelastic tests on a new concept dynamometric section model of the Messina suspension bridge, JWEIA, *92*, 2004, 441-462.

Masuyama Y. et al., 'Database of sail shapes vs sail performance and validation of numerical calculation for upwind condition', *18th Chesapeake Sailing Yacht Symposium- Annapolis*, March 2007

Milgram J. et al., 'Modelling IACC sail forces by combining measurements with CFD', *11th Chesapeake Sailing Yacht Symposium- Annapolis*, March 1993

Krebber B. Hochkirch K., 'Numerical investigation on the effects of trim for a yacht rig', *High Performance Yacht Design Conference Auckland*, 14-16-Feb. 2006

J. M. C. Campbell, & A. R. Claughton, 'Wind Tunnel Testing of Sailing Yacht Rigs', *13th HISVA symposium* – Amsterdam 1994

R. G. J. Flay, 'A twisted flow wind tunnel for testing yacht sails', *Journal of Wind Engineering and industrial Aerodynamics*, 63 (1996) 171-182

Fossati F. et al., 'Wind Tunnel Techniques for Investigation and Optimization of Sailing Yachts Aerodynamics', *High Performance Yacht Design Conference Auckland*, 14-16-Feb. 2006

Trucco, Verri, *Introductory techniques for 3D Computer Vision* (Englewood Cliffs, NJ, Prentice-Hall, 1998).

Hartley, Zisserman, *Multiple view geometry in Computer Vision*, Cambridge University Press, 2000.

Gonzales, Woods, *Digital Image Processing using Matlab* (Englewood Cliffs, NJ, Prentice-Hall, 2004)

Zhengyou Zhang, A Flexible New Technique for Camera Calibration, *Technical Report MSR-TR-98-71*, Microsoft Research, 1998

ISO, Guide to the Expression of Uncertainty in Measurement (GUM), 1995.

Cheli, F., Resta, F., Belloli, M., Rocchi, D. An experimental and numerical investigation on the aerodynamic response of a 1:300 full aeroelastic model of the Messina bridge, ICWE 12, Cairns Australia ,1-6 July 2007

N.P. Jones, R.H. Scanlan, Advances (and challenges) in the prediction of long-span bridge response to wind, Proc of Int. Symp. On Advances in Bridge Aerodynamics, Copenhagen, Denmark, May 1998, pp.59-85